



Published in final edited form as:

J Phys Chem B. 2011 May 19; 115(19): 6157–6165. doi:10.1021/jp109629v.

Orientation of Fluorescent Lipid Analog BODIPY-PC to Probe Lipid Membrane Properties: Insights from Molecular Dynamics Simulations

Kevin C. Song[†], Philip W. Livanec^{‡,§}, Jeffery B. Klauda^{||}, Krzysztof Kuczera^{‡,¶}, Robert C. Dunn^{‡,§}, and Wonpil Im^{†,‡,¶,*}

[†] Center for Bioinformatics, The University of Kansas, 2030 Becker Drive, Lawrence KS 66047, USA

[‡] Ralph N. Adams Institute for Bioanalytical Chemistry, The University of Kansas, 2030 Becker Drive, Lawrence KS 66047, USA

[§] Department of Chemistry, The University of Kansas, 2030 Becker Drive, Lawrence KS 66047, USA

[¶] Department of Molecular Biosciences, The University of Kansas, 2030 Becker Drive, Lawrence KS 66047, USA

^{||} Department of Chemical and Biomolecular Engineering, The University of Maryland, 2113 Chemical and Nuclear Engineering, College Park MD 20742 USA

Abstract

Single-molecule fluorescence measurements have been used to characterize membrane properties, and recently showed a linear evolution of the fluorescent lipid analog BODIPY-PC towards small tilt angles in Langmuir-Blodgett monolayers as the lateral surface pressure is increased. In this work, we have performed comparative molecular dynamics (MD) simulations of BODIPY-PC in DPPC (dipalmitoylphosphatidylcholine) monolayers and bilayers at three surface pressures (3, 10, and 40 mN/m) to explore 1) the microscopic correspondence between monolayer and bilayer structures, 2) the fluorophore's position within the membrane, and 3) the microscopic driving forces governing the fluorophore's tilting. The MD simulations reveal very close agreement between the monolayer and bilayer systems in terms of the fluorophore's orientation and lipid chain order, suggesting that monolayer experiments can be used to approximate bilayer systems. The simulations capture the trend of reduced tilt angle of the fluorophore with increasing surface pressure as seen in the experimental results, and provide detailed insights into fluorophore location and orientation, not obtainable in the experiments. The simulations also reveal that the enthalpic contribution is dominant at 40 mN/m resulting in smaller tilt angles of the fluorophore, and the entropy contribution is dominant at lower pressures resulting in larger tilt angles.

Keywords

lipid order parameters; membrane thickness; lipid chain interdigitation; tilting entropy

WONPIL@KU.EDU.

SUPPORTING INFORMATION AVAILABLE: Figure S1 shows the tilt angle probability distribution of BODIPY-PC fluorophore and DPPC acyl chains in bilayer and monolayer systems. Figure S2 illustrates the snapshots of lipid molecules near BODIPY-PC. Figure S3 shows tilt angle profiles of BODIPY dye molecules as a function of simulation time. Figure S4 illustrates a snapshot showing BODIPY-PC that has a tilt angle close to 180°. This material is available free of charge via the Internet at <http://pubs.acs.org>

INTRODUCTION

Lipid bilayer membranes are one of the essential and critical components in biological cells. Membranes participate in numerous important biological functions by interacting with certain proteins as well as serving as a barrier to the passage of polar molecules and ions.¹ Due to the difficulties associated with studying intact membranes quantitatively, model lipid membranes have been widely used to explore biological membrane properties.² These simplified models enable precise control over lipid components and experimental conditions such as temperature and surface pressure. As such, these studies have collectively provided detailed insights into overall membrane structure,³ phase behavior,⁴ and the influence of sterols.⁵ In addition, considerable efforts have been made to define the structural characteristic of lipid membranes such as lipid chain tilting,⁶ bilayer thickness,⁷ acyl chain order parameters,⁸ surface area per lipid,^{3, 7, 9} and compressibility.¹⁰ It has also been shown that molecular dynamics (MD) simulations can accurately model the lipid chain order, area per lipid, compressibility, and bilayer thickness.¹¹

DPPC (dipalmitoylphosphatidylcholine) is one of the most well studied lipid types, and previous studies have utilized x-ray diffraction with monolayers to examine lipid chain tilting.^{6a, b} Recently, single-molecule fluorescence measurements have provided new insights into DPPC chain tilting and order at different surface pressures in both monolayers and bilayers.^{6c, d} These studies utilized out-of-focus polarized total internal reflectance fluorescence microscopy (PTIRF-M) to characterize the orientation of the fluorescent lipid analog BODIPY-PC (Figure 1), doped into DPPC membranes. Fluorescent lipid analogs such as BODIPY-PC are widely used in the study of both model and intact membranes.¹² They are ubiquitous in the studies of phase partitioning and also for understanding dynamics using techniques such as fluorescence recovery after photobleaching (FRAP) and fluorescence correlation spectroscopy (FCS).¹³ For Langmuir-Blodgett monolayers, these PTIRF-M single-molecule measurements showed that the tilt angle of the fluorophore is sensitive to lateral surface pressure and addition of sterols.^{6c, d} As surface pressure is increased, a linear evolution towards smaller tilt angles was observed, indicating an increase in the acyl chain order. The tilt angle dependence on surface pressure was used to construct a calibration plot to find the equivalent surface pressure for bilayers.^{6c}

Although monolayer experiments provide more convenient control over membrane properties such as surface pressure, bilayers certainly offer a more realistic representation of biological membranes. While trends in the PTIRF-M single-molecule orientation measurements clearly reflect changes in membrane structure, several important, fundamental questions remain unanswered; 1) what is the microscopic correspondence between monolayer and bilayer structures, 2) where does the probe position within the membrane, and 3) what are the microscopic driving forces determining the orientation of the reporter dye at different surface pressures? To address these questions, we have performed a total of 1.5- μ s comparative MD simulations of DPPC monolayer and bilayer systems incorporating one BODIPY-PC molecule per leaflet at low (3 mN/m), medium (10 mN/m), and high (40 mN/m) lateral pressures. In addition, since the previous single-molecule PTIRF-M experiments^{6c, d} were done at room temperature, which is below the transition temperature of DPPC (323 K), we have done the measurements again at 323 K in order to directly compare with the simulation results. To the best of our knowledge, this is the first MD simulation work of the BODIPY dye in a membrane and the first attempt to directly compare MD simulations and single-molecule experimental approaches using BODIPY.

METHODS

BODIPY-PC parameters

In order to simulate BODIPY-PC in lipid membranes, we first created CHARMM topology and parameters of the BODIPY-PC molecule through the following steps. The first step involved parameterization of BODIPY molecule. The geometry optimization, vibrational frequency calculations, and CHELPG electrostatic potential fitting of atomic charges were performed at the HF/6-31G* level using GAUSSIAN03.¹⁴ The majority of the internal bonding force constants (bond stretching, angle bending, proper and improper torsions) were transferred from existing molecular fragments in the CHARMM force field.¹⁵ Fourteen parameters related to deformations around the boron center were optimized by fitting the CHARMM vibrational frequencies to GAUSSIAN03 results using the AFMM program,¹⁶ with 10,000 optimization cycles resulting in a root-mean-square fit of 82 cm⁻¹. The Lennard-Jones parameters for C, N, F and H atoms were transferred from analogous groups in the CHARMM force field.¹⁵ The LJ parameters for boron were taken from a sulfur atom (atom type S) in the CHARMM force field: $\epsilon -0.450$ kcal/mol and $R_{\min}/2 = 2.0$ Å. Similar LJ parameters for boron were used in a recent Boron-Nitride nanotube work with a slight difference of $R_{\min}/2$ of 0.3 Å: $\epsilon -0.453$ kcal/mol and $R_{\min}/2 = 1.69$ Å.¹⁷ In addition, since boron has a tetrahedral configuration, it has a limited direct interaction with solvent and lipids, and the detailed accuracy for the LJ terms may not be crucial in the BODIPY-PC case. These results were then used to create the topology and parameters for BODIPY-PC, with missing parameters transferred from analogous groups in the CHARMM force field.^{15a} The CHARMM topology and parameters of BODIPY-PC are available as Supporting Information (bodipy-pc-toppar.tar); a CHARMM input, bodipy-pc.inp, is provided to create a BODIPY-PC molecule.

Molecular dynamics simulations

Using the input scripts from the CHARMM-GUI Membrane Builder (www.charmm-gui.org),¹⁸ two BODIPY-PC molecules were inserted into the top and bottom leaflets of an equilibrated DPPC bilayer with 64 lipids on each leaflet, and the lipid system was solvated with 4635 water molecules, and 14 K⁺ and 14 Cl⁻ ions, corresponding to 0.15 M KCl solution (a total of 30853 atoms; Figure 2). The area per lipid was set to 64 Å², which corresponds to ~10 mN/m (medium lateral pressure). We assume that BODIPY-PC has the same lipid area as DPPC, given the structural similarity between the two molecules (Figure 1). Then, five independent simulation runs at this surface area were equilibrated for 200 ps with different initial velocity assignment. Each equilibrated bilayer system was used to build monolayers by switching the top and bottom half of the bilayer and by increasing the system size along the Z-axis to 140 Å to prevent the interaction between both leaflets through the periodic boundary conditions (Figure 2).

All calculations were performed in the *NPAT* (constant pressure, area, and temperature) ensemble¹⁹ at 323 K using the biomolecular simulation program CHARMM^{15a} with the C27r all-atom parameter set.²⁰ A time step of 2 fs was used with the SHAKE algorithm.²¹ We used the same options for non-bonded interactions in the input scripts provided by the CHARMM-GUI Membrane Builder;^{18a, 18c} the van der Waals interactions were smoothly switched off at 10–12 Å by a force switching function²² and electrostatic interactions were calculated using the particle-mesh Ewald (PME) method with a mesh size of about 1 Å for fast Fourier transformation, $\kappa = 0.34$ Å⁻¹, and a sixth-order B-spline interpolation.²³ For each of the independent monolayer and bilayer simulation runs, we performed 50-ns simulations including 3-ns equilibration.

To build the low-pressure (3 mN/m) and high-pressure (40 mN/m) monolayer and bilayer systems (Figure 2), we changed the surface area (64 \AA^2 per lipid $\approx 10 \text{ mN/m}$) of each equilibrated medium-pressure monolayer and bilayer system to 77 or 40 \AA^2 per lipid, respectively. The pressure isotherm for DPPC has been thoroughly studied, and changes in the area per molecule with surface pressure are well documented.^{6c, 24} The pressure change was done by gradually changing the system size by 1 \AA every 100 ps. We again carried out 50-ns simulations including 3-ns equilibration that consists of the system size adjustments. Therefore, we have performed 50-ns comparative MD simulations for a total of 30 simulation runs (5 monolayer and 5 bilayer runs each at low, medium, and high pressures).

Experimental Details

The previous single-molecule PTIRF-M experiments^{6c, d} were done at room temperature, which is below the transition temperature of DPPC (323 K). In this work, PTIRF-M measurements were done at 323 K in order to directly compare with the simulation results. In the measurements, the fluorescence from single BODIPY-PC dye molecules (Invitrogen Corporation, Carlsbad, CA, B3794) doped into DPPC membranes (Avanti Polar Lipids, Alabaster, AL) was individually analyzed to extract the three-dimensional orientation of the emission dipole.²⁵

For the preparation of monolayers, DPPC was dissolved in chloroform (1mg/ml stock solutions). The solutions were doped with $\sim 10^{-8}$ mol % BODIPY-PC reporter dye, and dispersed onto a subphase of ultra-pure water (18 M3) in a Langmuir-Blodgett trough (Type 611, Nima Technology, Coventry, England). For studies above the transition temperature of DPPC, a water circulator bath (Neslab RTE-140, Thermo Scientific, Waltham, MA) was used to circulate water under the Teflon surface of the LB trough to maintain a temperature of 323 ± 1 K. Once the lipid/chloroform mixture was dispersed on the subphase, the chloroform was allowed to evaporate for 15 minutes. DPPC monolayers were compressed at a speed of $100 \text{ cm}^2/\text{min}$ to approximately 45 mN/m and then expanded at a speed of $80 \text{ cm}^2/\text{min}$. The compression/expansion cycles were repeated twice to anneal the monolayer. The monolayer film was then compressed to each of the three pressures (3, 10, and 40 mN/m), held for approximately 15–20 minutes, and then transferred in a head-group down geometry onto a Piranha cleaned glass substrate at a dipping speed of 25 mm/min.

All films were imaged using a total internal reflection fluorescence microscope (TIRF-M) (Olympus IX71, Center Valley, PA) equipped with a 100x objective (1.45 NA achromat). The 514 nm line from an argon ion laser (Coherent Innova 70 Spectrum, Santa Clara, CA) was directed through half-wave and quarter-wave plates (Newport, Irvine, CA) to generate p-polarized excitation. Excitation was directed through the objective and fluorescence collected in an epifluorescence geometry with the optics defocused ~ 500 nm. As others have shown, defocusing the optics leads to distinct emission patterns in the single molecule fluorescence image that reflects the orientation of each molecule (see 6c, d and references therein). Analysis of the single molecule emission patterns enables both the polar and azimuthal angles to be extracted for each BODIPY-PC doped into the DPPC membranes. The fluorescence was filtered with a combination of a dichroic mirror and long pass filters (Chroma, Rockingham, VT) and imaged onto a CCD camera (Cascade 650, Roper Scientific, Tucson, AR). Image collection was controlled with Slidebook software (Version 4.2, Intelligent Imaging Innovations, Denver, CO) and analyzed using MatLab software (Natick, MA) (see references 6c, d for details). Such measurements, therefore, enable a direct comparison to be made between the single molecule orientation measurements and the single molecular simulations described above.

RESULTS AND DISCUSSION

Correspondence between Lipid Monolayers and Bilayers

To explore the microscopic correspondence between monolayer and bilayer structures, we first examined the BODIPY-PC orientation in the systems. Figure 3A shows the distribution of BODIPY-PC tilt angles (τ , the angle between the fluorophore vector in Figure 1 and the membrane normal) in the monolayer and bilayer simulation systems at three different surface pressures. The distributions reveal nearly identical structures between the monolayer and bilayer systems for each pressure. At high surface pressure, the fluorophore molecule is predominantly aligned normal to the membrane with most of the population having $\tau < 20^\circ$, which is well correlated with the tilt angles of lipid tails (Figures S1–2 in Supporting Information). A second peak around $40\text{--}50^\circ$ for the high-pressure bilayer system, which is missing in the monolayer results, is due to intermittent visits of dye molecules to tilted conformations during the simulations (Supporting Figure S3). The mean BODIPY-PC tilt angle increases as the pressure decreases and its distribution becomes broader for monolayers and bilayers. These results clearly illustrate that the dye molecule responds to the changes in the surrounding membrane environment such as surface pressure. Moreover, the tilt angle distributions of monolayers and bilayers behave similarly when different pressures are applied, and those of the corresponding monolayer and bilayer systems match quite well. This result indicates that monolayers can be used to approximate bilayer systems particularly with respect to at least lipid tilt and associated properties.

To explore the extent of the acyl chain order in the monolayer and bilayer systems, lipid chain order parameters ($|S_{cd}|$) were calculated for each pressure (Figure 4A). As expected, order parameters are highest for the high-pressure systems, i.e., the lipid chain order is increased as the lateral surface pressure increases. In fact, this observation is correlated with the bilayer thickness as a function of surface pressure (Figure 4B), i.e., the membrane thickness is increased as the lipid chain order increases. Such a correlation can be visualized in Figure 2. This result shows that as the surface pressure is increased, packing of the lipid molecules in the membranes becomes tighter, which is reflected in the small tilt angle distribution of the BODIPY-PC molecule (Figure 3A) and lipid tails (Supporting Figure S1). Moreover, there is a good agreement in $|S_{cd}|$ between corresponding monolayers and bilayers with only slight deviations in the low-pressure system. This again indicates similar structural properties for lipid monolayers and bilayers. The slight deviations with low pressure membranes appear to arise from the increased interdigitation (i.e., overlap) between the lipid acyl chains of each leaflet in the bilayers (Figure 5), which is absent in the monolayer systems.²⁶ With increased interdigitation, the nature of lipid-lipid interactions between the corresponding monolayer and bilayer systems becomes different in low-pressure systems; the lipid chains in bilayer systems are more ordered than in monolayer systems, which needs to be considered carefully in monolayer experiments.

BODIPY-PC Position in Membranes

In order to examine the position of the BODIPY-PC fluorophore within the membrane, we calculated the interaction partners of the fluorophore molecule in each system. As shown in Figure 6A, the fluorophore in BODIPY-PC predominantly interacts with lipid acyl chains at any given surface pressure, although the fluorophore's interaction with water and headgroup slightly increases as surface pressure decreases. It becomes clear that the BODIPY-PC molecule does change their orientation in response to the changes in the acyl chain properties through such extensive interactions with lipid acyl chains. To further examine and visualize the position of the fluorophore in the membrane, the density profiles of individual components in the system were calculated (Figure 7). The density profiles confirm that the dye almost entirely remains in the membrane hydrophobic region. Interestingly, although τ

and $|\tau - 180^\circ|$ are indistinguishable in experiments, MD simulations show that the BODIPY-PC dye explores tilt angles close to 180° intermittently at the low and medium pressures (Supporting Figures S3–4). Such visits to the head group region increase interactions of the dye with water and lipid head groups (Figure 6B), but these interactions diminish as the surface pressure increases due to a shift to smaller τ (Figure 6A).

Comparison with Experiments

Figure 3B shows the distributions of BODIPY-PC tilt angles from the single molecule fluorescence measurements of the dye molecules doped into DPPC monolayers at low and high surface pressures (see Experimental details in METHODS). A bimodal distribution in tilt angles is observed at both surface pressures, consistent with previous measurements done at room temperature.^{6c, d} At both pressures, large populations of molecules are observed oriented normal to the surface ($\tau < 10^\circ$) and in the plane of film ($\tau > 80^\circ$), with few oriented at intermediate angles. As also shown in Figure 3B, the MD simulations at low pressure reveal a broad distribution of tilt angles centered at large τ which sharpens and shifts to smaller τ at higher pressure. In both experiments and MD simulations, there is a clear trend of increased order in the system as the surface pressure is increased, despite a considerable difference between the simulated model and experimental conditions, such as experiments on supported membranes versus simulations of unsupported membranes. Unlike the experimental results, however, the MD simulations do not show a bimodal distribution in τ .

It is instructive to consider possible reasons for such discrepancy between simulation and experimental results. First, the characteristic bimodal distributions in the experimental results may arise from lipid phase coexistence, which is not captured in the relatively small membrane models used in the simulations.^{1, 27} Second, previous studies based on fluorescence quenching analysis²⁸ showed that BODIPY-PC similar to ours can have two distinct positions in membrane bilayers; one is close to the lipid head group/water interface, and the other is close to the bilayer center, although these experiments could not provide a detailed orientation of the BODIPY dye. Therefore, one can also envision another possibility that the bimodal distribution of the BODIPY dye tilt angle possibly arises from their distinct locations: small tilt angles from the BODIPY buried in the lipid chain and large tilt angles ($\tau \approx 90^\circ$) from the dye in/on the lipid head group.

While it is intractable to verify the influence of the lipid phase separation on the BODIPY orientation using atomistic MD simulations of the present system sizes, we have performed additional simulations to examine the influence of the dye locations on the BODIPY orientation. Such additional simulations were necessary because, while there is sufficient sampling of the dye orientation in the lipid chain region (Figures 7 and S3), it was not the case for the dye conformation in the region of the head group in the present simulations. Therefore, using the final structures (from three independent systems) at the medium pressure, we first performed restrained MD simulations by moving BODIPY's center of mass (Z_{dye}) from 3 Å to 24 Å (upper leaflet BODIPY-PC) and -3 Å to -24 Å (lower leaflet BODIPYPC) by 1 Å every 100 ps. We then performed 10-ns unrestrained (normal) MD simulations for the systems with $|Z_{\text{dye}}| = 3, 6, 9, 12, 15, 18, 21, \text{ and } 24$ Å in three independent systems.

As shown in Figures 8A, during the restrained MD simulations, BODIPY shows a clear tendency to have large tilt angles as it is forced to move to the lipid head group region ($|Z| = 19 \pm 5$). However, as shown in Figures 8B, most BODIPY molecules move back to the orientation/location shown in Figures 3 and 7, i.e., smaller tilt angles inside the lipid hydrophobic region; such an orientation/location appears to be an equilibrium one in the current BODIPY force field. While the current simulations cannot definitively resolve the origin of the bimodal distributions observed in the single molecule experiments, it is

suggestive that such distribution may result from the lipid phase separation than the distinct dye locations in the membranes. Nonetheless, it should be stressed that agreement between experiment and simulation shows a shift in the population of tilt angles towards smaller angles upon increase of surface pressure and demonstrates that such experiments can capture the changes occurring in the membrane structure.

Energetics of BODIPY-PC Tilting

While the current simulations cannot reproduce the experimental bimodal distribution of BODIPY tilt, it is still instructive to consider the energetics of BODIPY tilting in bilayers with different surface pressures because the simulations at least capture the trend of reduced tilt angle of the fluorophore with increasing surface pressure as seen in the experimental results. It has been shown that single-pass transmembrane helix tilting is governed by the intrinsic entropy from the helix precession around the membrane normal as well as specific helix-membrane interactions.²⁹ Using a similar approach, the mean interaction energy of BODIPY-PC with surrounding environments (i.e., lipid, water, and ions) was calculated as a function of τ . Assuming that the mean interaction energy is similar to the enthalpic contribution, Figure 9A shows that at low and medium pressures, the enthalpic contribution remains approximately constant as a function of τ . This demonstrates that the dye molecule tilting toward large tilt angles at these pressures (Figure 3A) is driven by the entropy contribution (Figure 9B) that represents the increased freedom of movement for the dye around the membrane normal, i.e., the accessible orientational space of the dye is reduced as τ decreases, which causes the entropy penalty associated with small tilt angles. However, at a high surface pressure, there is a significant interaction energy penalty associated with larger tilting of the dye due to tight packing of acyl chains. Thus, the enthalpic contribution becomes dominant and the dye prefers to stay at smaller tilt angles. This analysis reveals that the BODIPY-PC dye responds to the local environmental changes through detailed interplays between the enthalpic (dye-lipid interactions) and entropy (dye configurations) contributions.

CONCLUSION

To the best of our knowledge, we present the first MD simulation study of the BODIPY dye in a membrane, which has been used extensively in various biology experiments.¹²⁻¹³ The MD simulations of BODIPY-PC at three surface pressures reveal very close agreement between the monolayer and bilayer systems in terms of the dye orientations and lipid chain order. These observations suggest that monolayer experiments can be used to approximate bilayer systems at least for these and associated properties. In general, the simulations capture the trend towards normal oriented dyes with increasing surface pressure as seen in the single-molecule experimental results. In addition, the simulations provide detailed insights into dye location and orientation, which are not readily obtained in the experiments. Such comparisons provide a basis for understanding the recent single molecule measurements characterizing BODIPY-PC tilt angles in similar films. The simulations also provide insights into the microscopic driving forces governing the dye molecule tilting; the enthalpic contribution is dominant at high pressure conditions resulting in smaller tilt angles, and the entropy contribution is dominant at medium and low pressures resulting in larger tilt angles.

Finally, although the current simulations cannot definitively resolve the origin of the bimodal distributions observed in the single molecule experiments, the additional restrained/unrestrained MD simulations suggest that such distribution may result from the lipid phase separation than the distinct dye locations in the membranes. Further computational studies of this important dye molecule, such as free energy calculations as a function of the dye

orientation in different lateral pressures (representing different lipid phases), may elucidate the origin of the bimodal distributions observed in the single molecule experiments.

Supplementary Material

Refer to Web version on PubMed Central for supplementary material.

Acknowledgments

This work was supported by K-INBRE undergraduate scholarship from NIH P20 RR016475 (to KCS) and NSF MCB-0918374 (to WI). This research was also supported in part by NSF OCI-0503992 through TeraGrid resources provided by Purdue University.

References

1. van Meer G, Voelker DR, Feigenson GW. Membrane lipids: where they are and how they behave. *Nature Reviews Molecular Cell Biology*. 2008; 9(2):112–124.
2. Marsh D. Lateral pressure in membranes. *Biochim Biophys Acta*. 1996; 1286(3):183–223. [PubMed: 8982283]
3. Klauda JB, Kučerka N, Brooks BR, Pastor RW, Nagle JF. Simulation-based Methods for Interpreting X-ray Data from Lipid Bilayers. *Biophys J*. 2006; 90(8):2796–2807. [PubMed: 16443652]
4. (a) Hung WC, Lee MT, Chen FY, Huang HW. The condensing effect of cholesterol in lipid bilayers. *Biophys J*. 2007; 92(11):3960–3967. [PubMed: 17369407] (b) de Vries AH, Yefimov S, Marrink SJ. Molecular structure of the lecithin ripple phase. *Proc Natl Acad Sci U S A*. 2005; 102(15):5392–5396. [PubMed: 15809443]
5. (a) Marrink SJ, deVries AH, Harroun TA, Katsaras J, Wassall SR. Cholesterol Shows Preference for the Interior of Polyunsaturated Lipid Membranes. *J Am Chem Soc*. 2008; 130(1):10–11. [PubMed: 18076174] (b) Pan J, Mills TT, Tristram-Nagle S, Nagle JF. Cholesterol Perturbs Lipid Bilayers Nonuniversally. *Phys Rev Lett*. 2008; 100(19):198103. [PubMed: 18518492]
6. (a) Bringezu F, Majerowicz M, Wen S, Reuther G, Tan KT, Kuhlmann J, Waldmann H, Huster D. Membrane binding of a lipidated N-Ras protein studied in lipid monolayers. *Eur Biophys J*. 2007; 36(4–5):491–8. [PubMed: 17186235] (b) Wagner K, Brezesinski G. Modifying dipalmitoylphosphatidylcholine monolayers by n-hexadecanol and dipalmitoylglycerol. *Chem Phys Lipids*. 2007; 145(2):119–27. [PubMed: 17187768] (c) Livanec PW, Huckabay HA, Dunn RC. Exploring the Effects of Sterols in Model Lipid Membranes Using Single-Molecule Orientations. *J Phys Chem B*. 2009; 113(30):10240–10248. [PubMed: 19572622] (d) Livanec PW, Dunn RC. Single-Molecule Probes of Lipid Membrane Structure. *Langmuir*. 2008; 24(24):14066–14073. [PubMed: 19053664]
7. Nagle JF, Tristram-Nagle S. Structure of lipid bilayers. *Biochimica et Biophysica Acta-Reviews on Biomembranes*. 2000; 1469(3):159–195.
8. (a) Seelig A, Seelig J. The Dynamic Structure of Fatty Acyl Chains in a Phospholipid Bilayer Measured by Deuterium Magnetic Resonance. *Biochemistry*. 1974; 13(23):4839–4845. [PubMed: 4371820] (b) Seelig A, Seelig J. Bilayers of dipalmitoyl-3-sn-phosphatidylcholine conformational differences between the fatty acyl chains. *Biochim Biophys Acta*. 1975; 406:1–5. [PubMed: 1242107] (c) Douliez JP, Leonard A, Dufourc EJ. Restatement of Order Parameters in Biomembranes - Calculation of C-C Bond Order Parameters from C-D Quadrupolar Splittings. *Biophys J*. 1995; 68(5):1727–1739. [PubMed: 7612816] (d) Feller SE, Venable RM, Pastor RW. Computer simulation of a DPPC phospholipid bilayer: Structural changes as a function of molecular surface area. *Langmuir*. 1997; 13(24):6555–6561.
9. Kučerka N, Liu YF, Chu NJ, Petrache HI, Tristram-Nagle ST, Nagle JF. Structure of fully hydrated fluid phase DMPC and DLPC lipid bilayers using X-ray scattering from oriented multilamellar arrays and from unilamellar vesicles. *Biophys J*. 2005; 88(4):2626–2637. [PubMed: 15665131]
10. (a) Feller SE, Pastor RW. Constant surface tension simulations of lipid bilayers: The sensitivity of surface areas and compressibilities. *J Chem Phys*. 1999; 111(3):1281–1287. (b) Venable RM,

- Skibinsky A, Pastor RW. Constant surface tension molecular dynamics simulations of lipid bilayers with trehalose. *Mol Sim*. 2006; 32(10–11):849–855.(c) Poger D, Gunsteren WFV, Mark AE. A new force field for simulating phosphatidylcholine bilayers. *J Comput Chem*. 2010; 31(6): 1117–1125. [PubMed: 19827145] (d) Poger D, Mark AE. On the Validation of Molecular Dynamics Simulations of Saturated and cis-Monounsaturated Phosphatidylcholine Lipid Bilayers: A Comparison with Experiment. *Journal of Chemical Theory and Computation*. 2009; 6(1):325–336.(e) Rawicz W, Olbrich KC, McIntosh T, Needham D, Evans E. Effect of Chain Length and Unsaturation on Elasticity of Lipid Bilayers. 2000; 79(1):328–339.
11. Klauda JB, Venable RM, Freites JA, O'Connor JW, Tobias DJ, Mondragon-Ramirez C, Vorobyov I, Mackerell AD, Pastor RW. Update of the CHARMM All-Atom Additive Force Field for Lipids: Validation on Six Lipid Types. *J Phys Chem B*. 2010
 12. (a) Ariola FS, Mudaliar DJ, Walvick RP, Heikal AA. Dynamics imaging of lipid phases and lipid-marker interactions in model biomembranes. *Phys Chem Chem Phys*. 2006; 8(39):4517–29. [PubMed: 17047749] (b) Berezin MY, Achilefu S. Fluorescence lifetime measurements and biological imaging. *Chem Rev*. 2010; 110(5):2641–84. [PubMed: 20356094]
 13. (a) Gombos I, Steinbach GB, Pomozi I, Balogh A, Vamosi G, Gansen A, Laszlo G, Garab G, Matko J. Some new faces of membrane microdomains: A complex confocal fluorescence, differential polarization, and FCS imaging study on live immune cells. *Cytom Part A*. 2008; 73A(3):220–229.(b) Redman CA, Kusel JR. Distribution and biophysical properties of fluorescent lipids on the surface of adult *Schistosoma mansoni*. *Parasitology*. 1996; 113(Pt 2):137–43. [PubMed: 8786886] (c) Golebiewska U, Nyako M, Woturski W, Zaitseva I, McLaughlin S. Diffusion coefficient of fluorescent phosphatidylinositol 4,5-bisphosphate in the plasma membrane of cells. *Mol Biol Cell*. 2008; 19(4):1663–1669. [PubMed: 18256277]
 14. Frisch, MJ.; Schlegel, GWTHB.; Scuseria, GE.; Robb, MA.; Cheeseman, JR.; Montgomery, JA., Jr; Vreven, T.; Kudin, KN.; Burant, JC.; Millam, JM.; Iyengar, SS.; Tomasi, J.; Barone, V.; Mennucci, B.; Cossi, M.; Scalmani, G.; Rega, N.; Petersson, GA.; Nakatsuji, H.; Hada, M.; Ehara, M.; Toyota, K.; Fukuda, R.; Hasegawa, J.; Ishida, M.; Nakajima, T.; Honda, Y.; Kitao, O.; Nakai, H.; Klene, M.; Li, X.; Knox, JE.; Hratchian, HP.; Cross, JB.; Bakken, V.; Adamo, C.; Jaramillo, J.; Gomperts, R.; Stratmann, RE.; Yazyev, O.; Austin, AJ.; Cammi, R.; Pomelli, C.; Ochterski, JW.; Ayala, PY.; Morokuma, K.; Voth, GA.; Salvador, P.; Dannenberg, JJ.; Zakrzewski, VG.; Dapprich, S.; Daniels, AD.; Strain, MC.; Farkas, O.; Malick, DK.; Rabuck, AD.; Raghavachari, K.; Foresman, JB.; Ortiz, JV.; Cui, Q.; Baboul, AG.; Clifford, S.; Cioslowski, J.; Stefanov, BB.; Liu, G.; Liashenko, A.; Piskorz, P.; Komaromi, I.; Martin, RL.; Fox, DJ.; Keith, T.; Al-Laham, MA.; Peng, CY.; Nanayakkara, A.; Challacombe, M.; Gill, PMW.; Johnson, B.; Chen, W.; Wong, MW.; Gonzalez, C.; Pople, JA. GAUSSIAN03. Gaussian Inc; 2004.
 15. (a) Brooks BR, Brooks CL, Mackerell AD, Nilsson L, Petrella RJ, Roux B, Won Y, Archontis G, Bartels C, Boresch S, Caffisch A, Caves L, Cui Q, Dinner AR, Feig M, Fischer S, Gao J, Hodoseck M, Im W, Kuczera K, Lazaridis T, Ma J, Ovchinnikov V, Paci E, Pastor RW, Post CB, Pu JZ, Schaefer M, Tidor B, Venable RM, Woodcock HL, Wu X, Yang W, York DM, Karplus M. CHARMM: The Biomolecular Simulation Program. *J Comput Chem*. 2009; 30(10):1545–1614. [PubMed: 19444816] (b) Mackerell AD Jr. Empirical force fields for biological macromolecules: overview and issues. *J Comput Chem*. 2004; 25(13):1584–604. [PubMed: 15264253]
 16. Vaiana AC, Schulz A, Wolfrum J, Sauer M, Smith JC. Molecular mechanics force field parameterization of the fluorescent probe rhodamine 6G using automated frequency matching. *J Comput Chem*. 2003; 24(5):632–9. [PubMed: 12632478]
 17. Hilder TA, Yang R, Ganesh V, Gordon D, Bliznyuk A, Rendell AP, Chung SH. Validity of current force fields for simulations on boron nitride nanotubes. *Micro Nano Lett*. 2010; 5(2):150–156.
 18. (a) Jo S, Kim T, Im W. Automated Builder and Database of Protein/Membrane Complexes for Molecular Dynamics Simulations. *PLoS ONE*. 2007; 2(9):e880. [PubMed: 17849009] (b) Jo S, Kim T, Iyer VG, Im W. CHARMM-GUI: a web-based graphical user interface for CHARMM. *J Comput Chem*. 2008; 29(11):1859–65. [PubMed: 18351591] (c) Jo S, Lim JB, Klauda JB, Im W. CHARMM-GUI Membrane Builder for mixed bilayers and its application to yeast membranes. *Biophys J*. 2009; 97(1):50–8. [PubMed: 19580743]
 19. Feller SE, Pastor RW. On simulating lipid bilayers with an applied surface tension: Periodic boundary conditions and undulations. *Biophysical Journal*. 1996; 71(3):1350–1355. [PubMed: 8874010]

20. (a) Klauda JB, Brooks BR, MacKerell AD Jr, Venable RM, Pastor RW. An ab initio study on the torsional surface of alkanes and its effect on molecular simulations of alkanes and a DPPC bilayer. *J Phys Chem B*. 2005; 109(11):5300–11. [PubMed: 16863197] (b) Klauda JB, Pastor RW, Brooks BR. Adjacent gauche stabilization in linear alkanes: implications for polymer models and conformational analysis. *J Phys Chem B*. 2005; 109(33):15684–6. [PubMed: 16852989]
21. Ryckaert JP, Ciccotti G, Berendsen HJC. Numerical-Integration of Cartesian Equations of Motion of a System with Constraints - Molecular-Dynamics of N-Alkanes. *J Comput Phys*. 1977; 23(3): 327–341.
22. (a) Brooks CL III, Pettitt BM, Martin K. Structural and energetic effects of truncating long ranged interactions in ionic and polar fluids. *The Journal of Chemical Physics*. 1985; 83(11):5897–5908. (b) Steinbach PJ, Brooks BR. New spherical-cutoff methods for long-range forces in macromolecular simulation. *Journal of computational chemistry*. 1994; 15(7):667–683.
23. Essmann U, Perera L, Berkowitz ML, Darden T, Lee H, Pedersen LG. A smooth particle mesh Ewald potential. *J Chem Phys*. 1995; 103:8577–8592.
24. McConnell HM, Tamm LK, Weis RM. Periodic Structures in Lipid Monolayer Phase-Transitions. *P Natl Acad Sci USA*. 1984; 81(10):3249–3253.
25. (a) Bartko AP, Dickson RM. Imaging three-dimensional single molecule orientations. *J Phys Chem B*. 1999; 103(51):11237–11241. (b) Bartko AP, Dickson RM. Three-dimensional orientations of polymer-bound single molecules. *J Phys Chem B*. 1999; 103(16):3053–3056. (c) Forkey JN, Quinlan ME, Goldman YE. Measurement of single macromolecule orientation by total internal reflection fluorescence polarization microscopy. *Biophys J*. 2005; 89(2):1261–1271. [PubMed: 15894632] (d) Patra D, Gregor I, Enderlein J. Image analysis of defocused single-molecule images for three-dimensional molecule orientation studies. *J Phys Chem A*. 2004; 108(33):6836–6841. (e) Toprak E, Enderlein J, Syed S, McKinney SA, Petschek RG, Ha T, Goldman YE, Selvin PR. Defocused orientation and position imaging (DOPI) of myosin V. *Proc Natl Acad Sci*. 2006; 103(17):6495–6499. [PubMed: 16614073]
26. Kaiser RD, London E. Determination of the depth of BODIPY probes in model membranes by parallax analysis of fluorescence quenching. *Biochimica Et Biophysica Acta-Biomembranes*. 1998; 1375(1–2):13–22.
27. Risselada HJ, Marrink SJ. The molecular face of lipid rafts in model membranes. *Proceedings of the National Academy of Sciences*. 2008; 105(45):17367–17372.
28. Kaiser RD, London E. Determination of the depth of BODIPY probes in model membranes by parallax analysis of fluorescence quenching. *Biochim Biophys Acta*. 1998; 1375(1–2):13–22. [PubMed: 9767081]
29. (a) Lee J, Im W. Transmembrane Helix Tilting: Insights from Calculating the Potential of Mean Force. *Phys Rev Lett*. 2008; 100:018103. [PubMed: 18232823] (b) Kim T, Im W. Revisiting Hydrophobic Mismatch with Free Energy Simulation Studies of Transmembrane Helix Tilt and Rotation. *Biophysical Journal*. 2010; 99(1):175–183. [PubMed: 20655845] (c) Lee JY, Im WP. Restraint potential and free energy decomposition formalism for helical tilting. *Chem Phys Lett*. 2007; 441(1–3):132–135.

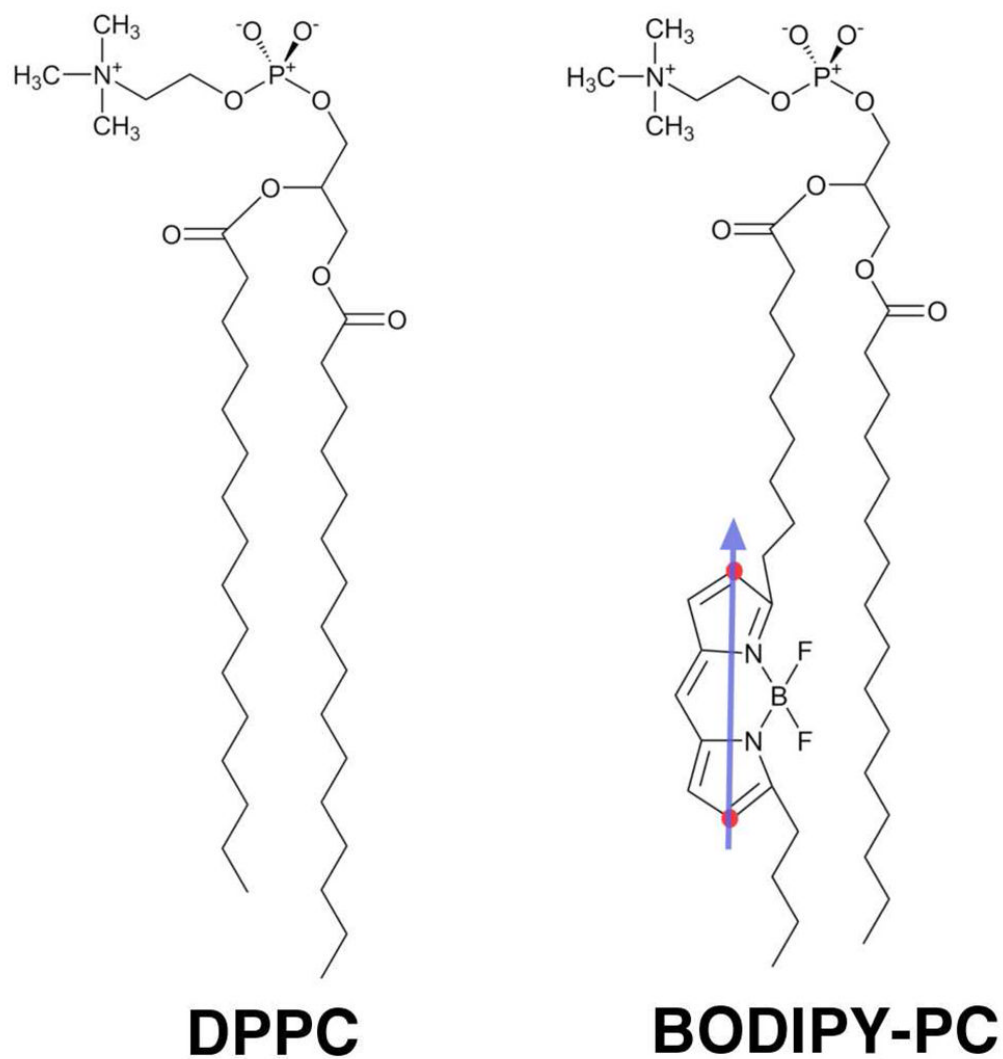


Figure 1. DPPC and BODIPY-PC with the fluorophore vector (between the two red carbons) to define its orientation.

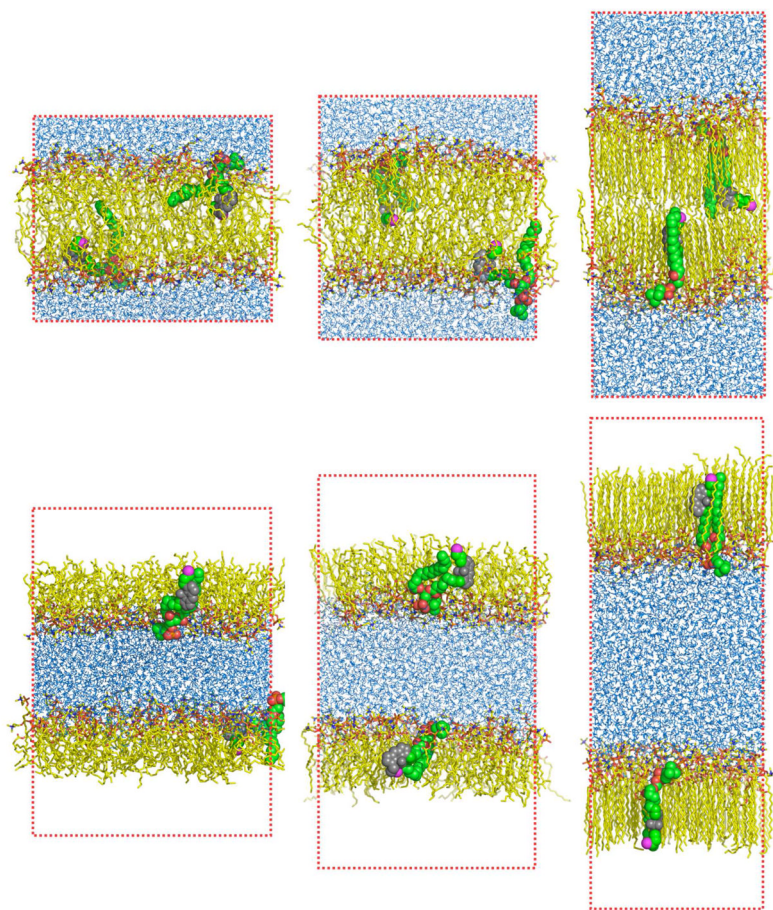


Figure 2. Molecular systems of bilayer (top) and monolayer (bottom) systems at 3 mN/m (low pressure, left), 10 mN/m (medium pressure, middle), 40 mN/m (high pressure, right). The red dashed box represents each system size. BODIPY-PC molecules are shown in space filling with gray for the fluorophore and magenta for the last carbon atom in the lipid tail with the fluorophore.

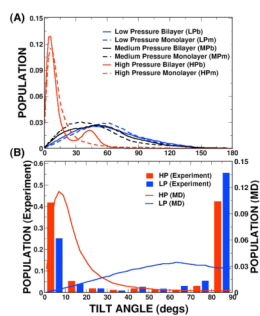


Figure 3. (A, B) Distributions of BODIPY-PC tilt angle from simulations and its comparison with experiments. In (B), the MD monolayer results are plotted from 0° to 90° after re-weighting because τ and $|\tau - 180^\circ|$ are indistinguishable in the experiments.

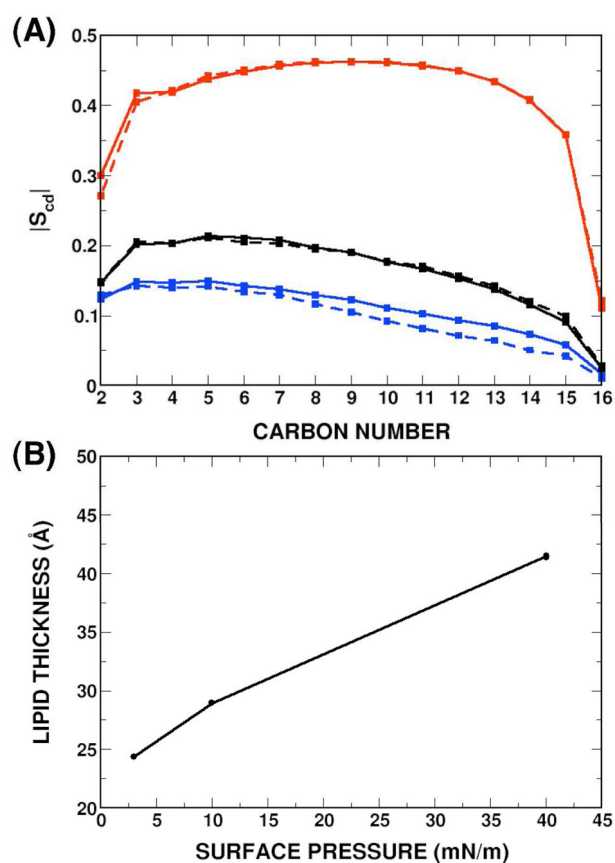


Figure 4.

(A) Lipid chain order parameters ($|S_{cd}|$) from simulations: $S_{cd} = \langle 3\cos^2\theta - 1 \rangle / 2$, where θ is the angle between the C-H bond vector and the Z-axis (membrane normal). The line schemes are the same as in Fig. 3A. (B) The bilayer thickness as a function of surface pressure. Each point represents the average bilayer thickness of 5 different bilayer systems at corresponding surface pressures. The bilayer thickness is measured as the average distance between the C2 carbon atoms in the top and bottom leaflets. The error bars are similar to the symbol size and are too small to be seen.

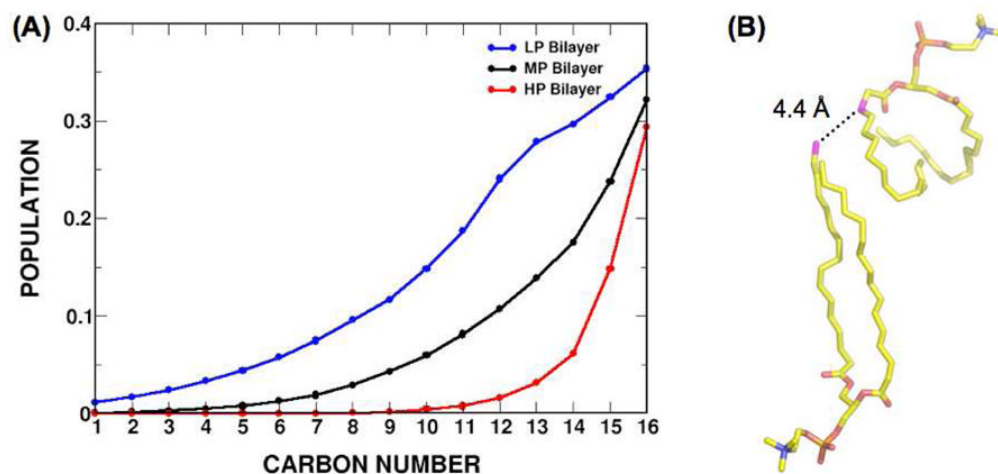


Figure 5.

(A) Distributions of interdigitation propensity as a function of acyl chain carbon number at three different pressures. The interdigitation population at each carbon represents its chance to have any close contact (within 4.5 Å) with any carbons in the opposite leaflet. For example, the probability for C₁₀ to interact with acyl carbons in the opposite leaflet increases from almost zero at the high pressure to ~5% and ~15% at the medium and low pressures, respectively. (B) A molecular picture showing the contact of C₁₆ carbon at the bottom leaflet to C₃ carbon at the upper leaflet.

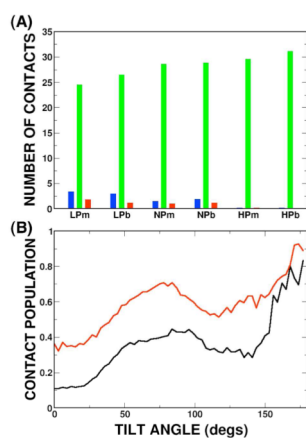


Figure 6. (A) Average numbers of water (blue), lipid chains (black), and head groups (red) within 4.5 Å of the fluorophore. (B) The probability distribution of having water (red) and lipid head group (black) as interacting partners (within 4.5 Å) of the dye molecule as a function of the dye tilt angle in the medium-pressure systems.

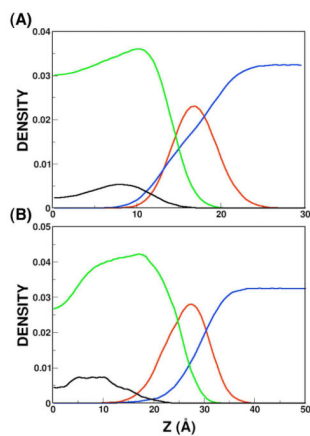


Figure 7. The number density of the BODIPY-PC fluorophore (black), lipid acyl chains (green), lipid head groups (red), and water (blue) for (A) low and (B) high lateral pressure systems. For clarity, the density of BODIPY-PC is scaled by 10.

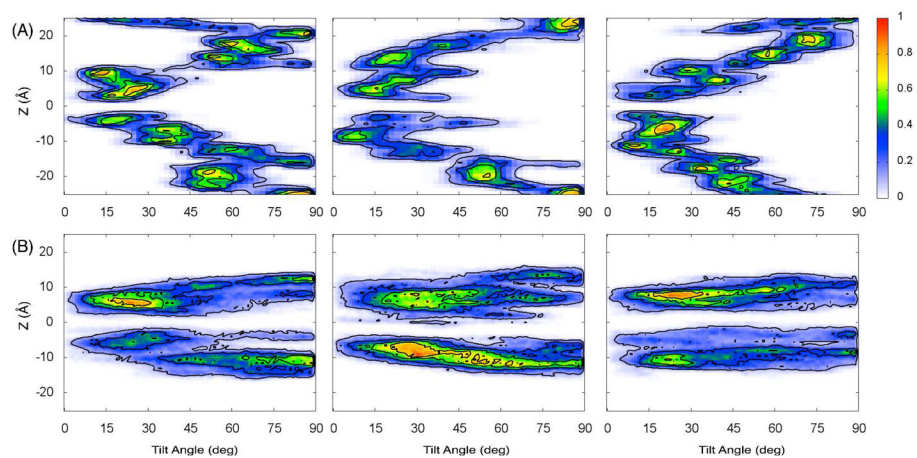


Figure 8. Two-dimensional distributions as a function of the dye tilt angle and the center of mass Z -position for (A) the initial restrained MD runs and (B) the final 2-ns production for three independent systems (in each row) at the medium lateral pressure. The color bars indicate the normalized population.

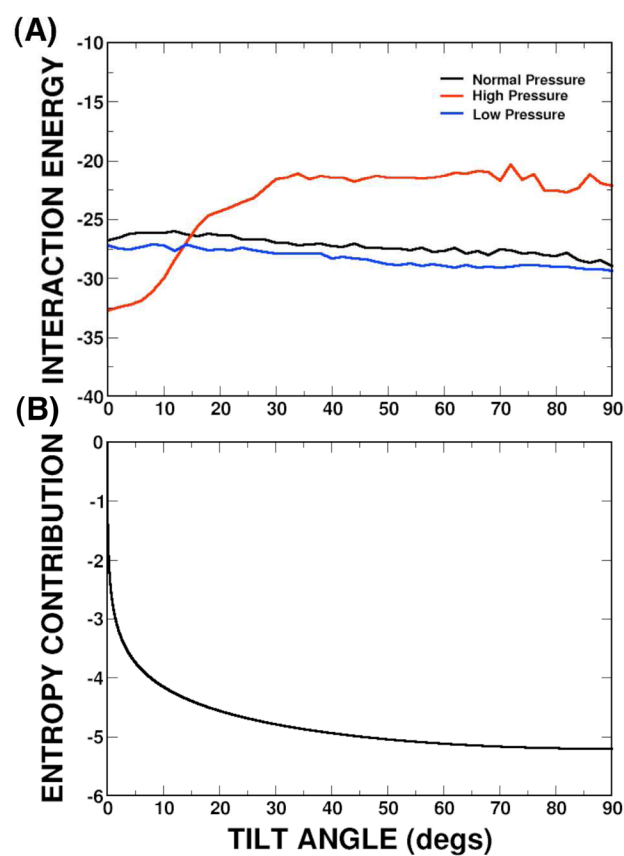


Figure 9. The energy profiles (in kcal/mol) of (A) interaction between the BODIPY-PC dye and surrounding environments, and (B) the entropy contribution as a function of the dye's τ . For clarity, the standard deviation in the interaction energy (± 2.5 kcal/mol) is not shown. The entropy contribution was calculated by $-k_B T \ln |\sin(\tau)|$ starting from $\tau = 0.01^\circ$ (the smallest τ observed in the simulations).^{29a}